

Asteroids in the Inner Solar System I – Existence

S.A. Tabachnik^{1,2} and N.W. Evans¹

¹ *Theoretical Physics, 1 Keble Rd, Oxford, OX1 3NP*

² *Princeton University Observatory, Princeton, NJ 08544-1001, USA*

ABSTRACT

Ensembles of in-plane and inclined orbits in the vicinity of the Lagrange points of the terrestrial planets are integrated for up to 100 million years. The integrations incorporate the gravitational effects of Sun and the eight planets (Pluto is neglected). Mercury is the least likely planet, as it is unable to retain tadpole orbits over 100 million year timescales. Mercurian Trojans probably do not exist, although there is evidence for long-lived, corotating horseshoe orbits with small inclinations. Both Venus and the Earth are much more promising, as they possess rich families of stable tadpole and horseshoe orbits. Our survey of Trojans in the orbital plane of Venus is undertaken for 25 million years. Some 40% of the survivors are on tadpole orbits. For the Earth, the integrations are pursued for 50 million years. The stable zones in the orbital plane are larger for the Earth than for Venus, but fewer of the survivors ($\sim 20\%$) are tadpoles. Both Venus and the Earth also have regions in which inclined test particles can endure near the Lagrange points. For Venus, only test particles close to the orbital plane ($i \lesssim 16^\circ$) are stable. For the Earth, there are two bands of stability, one at low inclinations ($i \lesssim 16^\circ$) and one at moderate inclinations ($24^\circ \lesssim i \lesssim 34^\circ$). The inclined test particles that evade close encounters are primarily moving on tadpole orbits. Two Martian Trojans (5261 Eureka and 1998 VF31) have been discovered over the last decade and both have orbits moderately inclined to the ecliptic (20.3° and 31.3° respectively). Our survey of in-plane test particles near the Martian Lagrange points shows no survivors after 60 million years. Low inclination test particles do not persist, as their inclinations are quickly increased until the effects of a secular resonance with Jupiter cause de-stabilisation. Numerical integrations of inclined test particles for timespans of 25 million years show stable zones for inclinations between 14° and 40° . However, there is a strong linear resonance with Jupiter which destabilises a narrow band of inclinations at $\sim 29^\circ$. Both 5261 Eureka and 1998 VF31 lie deep within the stable zones, which suggests they may be of primordial origin.

Key words: Solar System: general – minor planets, asteroids – planets and satellites: individual: Mercury, Venus, the Earth, Mars

1 INTRODUCTION

Lagrange’s (1772) triangular solution of the three body problem was long thought to be just an elegant mathematical curiosity. The three bodies occupy the vertices of an equilateral triangle. Any two of the bodies trace out elliptical paths with the same eccentricity about the third body as a focus (see e.g., Whittaker 1904, Pars 1965). The detection of 588 Achilles near Jupiter’s Lagrange point in 1906 by Wolf changed matters. This object librates about the Sun-Jupiter L_4 Lagrange point, which is 60° ahead of the mean orbital longitude of Jupiter (e.g., Érdi 1997). About 470 Jovian Trojans are now known (see “<http://cfa-www.harvard.edu/iau/lists/Trojans.html>”), though the total population exceeding 15 km in diameter may be as high as ~ 2500 (Shoemaker, Shoemaker & Wolfe 1989; French et

al. 1989). Roughly 80% of the known Trojans are in the L_4 swarm. The remaining 20% librate about the L_5 Lagrange point, which trails 60° behind the mean orbital longitude of Jupiter. There are also Trojan configurations amongst the Saturnian moons. The Pioneer 11 and the Voyager 1 and 2 flybys of Saturn discovered five small moons on tadpole or horseshoe orbits. The small moon Helene librates about the Saturn-Dione L_4 point. The large moon Tethys has two smaller Trojan moons called Telesto and Calypso, one of which librates about the Saturn-Tethys L_4 and the other about the Saturn-Tethys L_5 points. Finally, the two small moons Janus and Epimetheus follow horseshoe orbits co-orbiting with Saturn (see e.g., Smith et al. 1983; Yoder et al. 1983; Yoder, Synnott & Salo 1989). Another example of a Trojan configuration closer to home is provided by the ex-

arXiv:astro-ph/0005400v1 19 May 2000

tensive dust clouds in the neighbourhood of the L_5 point of the Earth-Moon system claimed by Winiarski (1989).

This paper is concerned with the existence of coorbiting asteroids near the triangular Lagrange points of the four terrestrial planets. For non-Jovian Trojans, the disturbing forces due to the other planets are typically larger than those caused by the primary planet itself. For this reason, it was formerly considered unlikely that long-lived Trojans of the terrestrial planets could survive. Over the past decade, two lines of evidence have suggested that this reasoning is incorrect. The first is the direct discovery of inclined asteroids librating about the Sun-Mars L_5 Lagrange point. The second is numerical integrations, which have steadily increased in duration and sophistication.

The first non-Jovian Trojan asteroid, 5261 Eureka, was discovered by Holt & Levy (1990) near the L_5 point of Mars. Surprisingly, the orbit of 5261 Eureka is inclined to the plane of the ecliptic by 20.3° . The determination of Eureka's orbital elements and a preliminary analysis of its orbit were published in Mikkola et al. (1994). Numerical integrations were performed for several dozen Trojan test particles with different initial inclinations for ~ 4 Myr by Mikkola & Innanen (1994), who claimed that long-term stability of Martian Trojans was possible only in well-defined inclination windows, namely $15^\circ \leq i \leq 30^\circ$ and $32^\circ \leq i \leq 44^\circ$ with respect to Jupiter's orbit. The discovery of a second Mars Trojan, 1998 VF31, soon followed (see e.g., *Minor Planet Circular 33763*; Tabachnik & Evans 1999). Perhaps the most important point to take from the observational discoveries is that if a comparatively puny body like Mars possesses Trojans, it is quite likely indeed that the more massive planets also harbour such satellites.

The main argument for the possible existence of Trojans of the Earth, Venus and Mercury comes from numerical test particle surveys. Much of the credit for reviving modern interest in the problem belongs to Zhang & Innanen (1988a,b,c). Using the framework of the planar elliptic restricted four and five-body problem, their integrations extended from 2000 to 10^5 years, though their model was not entirely self-consistent as mutual interactions between the planets were not taken into account. Further important results on the stability of the Trojans of the terrestrial planets were obtained in a series of papers by Mikkola & Innanen (1990, 1992, 1994, 1995). The orbits of the planets from Venus to Jupiter were computed at first using a Bulirsch-Stoer integration and later with a Wisdom-Holman (1991) symplectic integrator. In the case of Mercury, test particles placed at the Lagrange point exhibited a strongly unstable behaviour rather rapidly. Conversely, the mean librational motion of all the Trojan test particles near Venus and the Earth's Lagrange points appeared extremely stable. Thus far, the longest available integrations are the 6 Myr survey of test particles near the triangular L_4 point of Venus and the Earth (Mikkola & Innanen 1995). The initial inclinations ranged from 0° to 40° with respect to the orbital plane of the primary planet. The Trojans of Venus and the Earth persisted on stable orbits for small inclinations ($i \leq 18^\circ$ and $i \leq 11^\circ$ respectively).

These lines of reasoning suggest that a complete survey of the Lagrange points of the terrestrial planets is warranted. It is the purpose of the present paper to map out the zones in which coorbital asteroids of the terrestrial planets

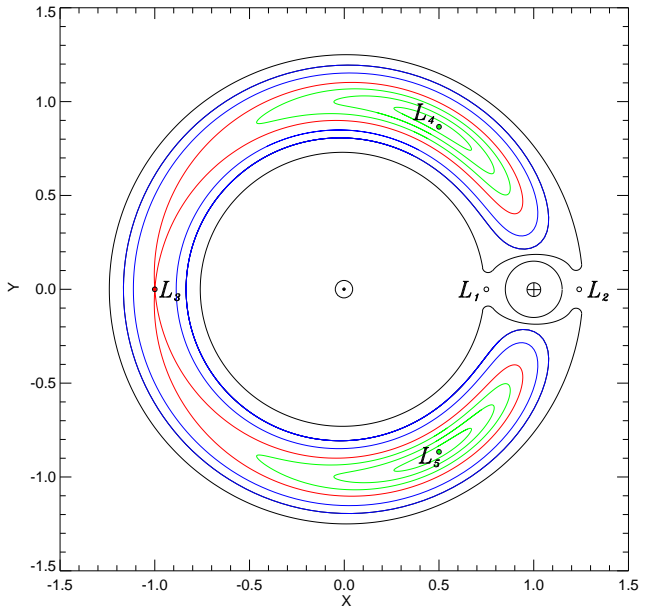


Figure 1. The positions of the five Lagrange points for the three body system in a corotating frame. There are two type of planar, coorbiting orbits – the tadpoles and the horseshoes. Tadpole orbits are shown in green and librate about either the leading L_4 or trailing L_5 Lagrange points. Horseshoe orbits are shown in blue and perform a double libration about both L_4 and L_5 . The orbits are based on numerical data for the case of the Sun, the Earth and an asteroid, but the difference in semimajor axis of the asteroid and the planet has been magnified by a factor of 40 for clarity. The dividing separatrix or orbit of infinite period is shown in red. The boundaries of the coorbital region are shown as full lines. They are schematic and correspond to bounding positions limited by L_1 and L_2 , which are themselves arbitrarily located. The satellite régime occupies a sphere around the planet.

can survive for timescales up to 100 million years. Section 2 provides a theoretical introduction to the dynamics of coorbital satellites within the framework of the elliptic restricted three body problem. Our fully numerical survey is discussed in Section 3 and takes into account the effects of all the planets (except Pluto), as well as the most important post-Newtonian corrections and the quadrupole moment of the Moon. The results of the survey are presented for each of the terrestrial planets in Sections 4 to 7 (Mercury, Venus, the Earth, and Mars). Finally, a companion paper in this issue of *Monthly Notices* discusses the observable properties of the asteroids.

2 THEORETICAL FRAMEWORK

Consider the restricted three-body problem, defined by a system of two massive bodies on Keplerian orbits attracting a massless test particle that does not perturb them in return. The five Lagrange points are the stationary points of the effective potential (e.g., Danby 1988). The collinear Lagrange points L_1 , L_2 and L_3 are unstable, whereas the triangular Lagrange points L_4 and L_5 form equilateral triangles with the two massive bodies, as illustrated in Fig. 1. Motion around L_4 and L_5 can be stable. The planar orbits

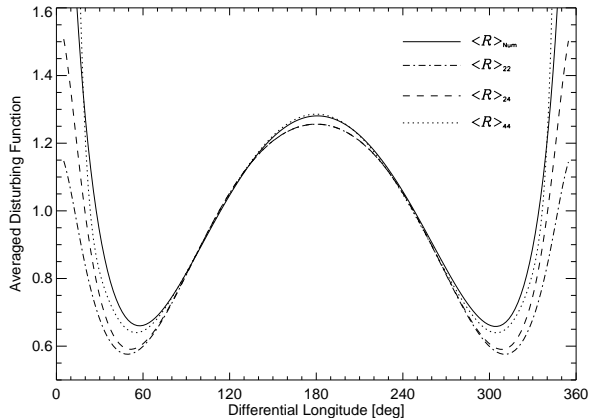


Figure 2. The averaged disturbing function (4) plotted as a function of differential longitude ϕ . The figure shows approximations carried out to second order in inclination and eccentricities $\langle R \rangle_{22}$, second order in inclination and fourth order in eccentricity $\langle R \rangle_{24}$ and fourth order in both quantities $\langle R \rangle_{44}$. They are compared to the numerically evaluated averaged disturbing function $\langle R \rangle_{\text{Num}}$.

Planet	L_4	L_5	ϕ_*
Mercury	59.822°	300.178°	25.736°
Venus	60.000°	300.000°	23.908°
Earth	59.999°	300.001°	23.917°
Mars	59.964°	300.036°	24.266°

Table 1. The angular positions of the Lagrange points as inferred from (4) for each of the terrestrial planets. The asteroidal orbit is assumed to have vanishing inclination and argument of pericentre. Note that the Lagrange points are displaced only slightly from their classical values. Also recorded is the angular position of the separatrix, which physically represents the minimum differential longitude that can be reached by the tadpole orbits.

that corotate with a planet are classified as either tadpoles or horseshoes. Tadpole orbits perform a simple libration about either the Lagrange point L_4 or L_5 , whereas the horseshoes perform a double libration about both L_4 and L_5 . The tadpole and horseshoe orbits are divided by a separatrix, which corresponds to an orbit of infinite period that passes through L_3 . On average, both tadpoles and horseshoes move about the Sun at the same rate as the parent planet.

It is helpful to develop an approximate treatment of coorbital motion. Within the framework of the elliptic restricted problem of three bodies (Sun, planet and asteroid), the Hamiltonian of the asteroid in a non-rotating heliocentric coordinate system reads:

$$H = -\frac{k^2}{2a} - m_p k^2 R, \quad (1)$$

where m_p is the mass of the planet in Solar masses and k is the Gaussian gravitational constant. The disturbing function R is defined by (e.g., Danby 1988)

$$R = \frac{1}{(r^2 + r_p^2 - 2rr_p \cos S)^{1/2}} - \frac{r \cos S}{r_p^2}. \quad (2)$$

Here, the radius vector r and r_p refer to the asteroid and the planet respectively, S being the elongation of the asteroid from the parent planet. Following Brouwer & Clemence (1961), $\cos S$ can be expressed in function of the mutual inclination of the two orbits i , the true anomalies ν and ν_p , the argument of perihelion ω and the longitude of the ascending node Ω of the asteroid:

$$\begin{aligned} \cos S &= \cos^2 \frac{i}{2} \cos(\nu - \nu_p + \omega + \Omega) \\ &+ \sin^2 \frac{i}{2} \cos(\nu + \nu_p + \omega - \Omega). \end{aligned} \quad (3)$$

The disturbing function is then expressed in terms of the mean synodic longitudes $\lambda_p = M_p$ and $\lambda = M + \omega + \Omega$. Here, M_p and M are the mean anomalies of the planet and asteroid. In other words, we are using a coordinate system for which (x, y) lies in the orbital plane of Mars and the x -axis points towards Mars' perihelion. The disturbing function is expanded to second order in the eccentricities and to fourth order in the inclination. Finally, we make a change of variables $\phi = \lambda_p - \lambda$ and average R over the mean anomaly of the planet M_p :

$$\langle R \rangle = \frac{1}{2\pi} \int_0^{2\pi} R dM_p = U_0 + U_2 + O(e^3, e_p^3, i^5). \quad (4)$$

The zeroth order term in the averaged disturbing function is

$$U_0 = \frac{1}{(a^2 + a_p^2 - 2aa_p \cos^2 \frac{i}{2} \cos \phi)^{1/2}} - \frac{a}{a_p} \cos^2 \frac{i}{2} \cos \phi. \quad (5)$$

The term that is second order in the eccentricities and inclinations has three parts

$$\begin{aligned} U_2 &= U_{2,0} + \frac{U_{2,3}}{(a^2 + a_p^2 - 2aa_p \cos^2 \frac{i}{2} \cos \phi)^{3/2}} \\ &+ \frac{U_{2,5}}{(a^2 + a_p^2 - 2aa_p \cos^2 \frac{i}{2} \cos \phi)^{5/2}}, \end{aligned} \quad (6)$$

where $U_{2,0}$, $U_{2,3}$ and $U_{2,5}$ are given in Appendix A. Still lengthier expressions accurate to the fourth order in the eccentricities and inclinations are given in Tabachnik (1999). It is interesting to note that the second order expressions depend only on the longitude of perihelion, while the fourth order contains terms depending on both the longitude of perihelion and the longitude of the ascending node. Some of these averaged disturbing functions are shown in Fig. 2 and compared to the numerically computed and averaged disturbing function $\langle R \rangle_{\text{Num}}$.

For small and moderate inclinations, $\langle R \rangle$ has a double-welled structure. The libration about the Lagrange points can be viewed as the trapping of the test particle in the well, with the tadpole orbits located in the deeper part of the well and the horseshoe orbits in the shallower part. The two orbital families are divided by a separatrix. The slight eccentricities and inclinations of the planets cause small deviations of the Lagrange points from their classical values (c.f. Namouni & Murray 1999). These deviations can be calculated by finding the local minima of the secular potential (4). The results for each terrestrial planet are recorded in Table 1.

The position of the separatrix is found by locating the local maximum of the secular potential (4). The separatrix terminates at a differential longitude from the planet ϕ_* . This angle is the closest any tadpole orbit can come to

the planet. In the restricted circular problem, this angle is $\phi_* = 2\text{asin}(\frac{1}{\sqrt{2}} - \frac{1}{2}) = 23.906^\circ$ (see e.g., Brown & Shook 1933). The deviation from this classical value caused by the eccentricity and inclination of the planets is also recorded in Table 1.

The secular potential (4) can also be used to work out the approximate period P of small angle librations about the Lagrange points. For simplicity, we take only the zeroth order term (5) with $a = a_p$ and obtain the minimum of the secular potential at

$$\phi = \text{acos}\left(\frac{1}{2\cos^2\frac{i}{2}}\right). \quad (7)$$

The period of small librations about this minimum is

$$P = \frac{2}{3} \frac{P_p}{\sqrt{m_p(4\cos^4(\frac{i}{2}) - 1)}} \quad (8)$$

where P_p is the orbital period of the planet. The period of libration increases with increasing inclination.

Expansion of the disturbing function is a good guide to the dynamics provided the inclinations and eccentricities are low or moderate. At high inclinations and eccentricities, the classification of the corotating orbits has only recently been undertaken by Namouni (1999).

3 NUMERICAL METHOD

For each of the terrestrial planets, we carry out numerical surveys of in-plane and inclined corotating orbits. Section 3.1 introduces the integration method, while Section 3.2 discusses the numerical procedure.

3.1 Mixed Variable Symplectic Integrators

Our model includes all the planets (except Pluto whose contribution is negligible in the inner Solar System). The asteroids are represented as test particles with infinitesimal mass. They are perturbed by the planets but they do not perturb them in return.

The orbits of the planets are integrated using a mixed variable symplectic integrator scheme (Wisdom & Holman 1991; Kinoshita, Yoshida & Nakai 1991) with individual time steps (Saha & Tremaine 1994) which takes into account post-Newtonian corrections and the quadrupole moment of the Sun's attraction on the barycentre of the Earth-Moon system (Quinn, Tremaine & Duncan 1991). The two latter contributions must be included for calculations in the inner Solar System, whereas the cumulative effect of the asteroids, satellites, galactic tidal acceleration, passing stars, solar mass loss and oblateness is believed to be smaller than $\sim 10^{-10}$ and is neglected (Quinn et al. 1991). Mixed variable symplectic integrators exploit the fact that the Hamiltonian written in Jacobi coordinates (Plummer 1960; Wisdom & Holman 1991) is dominated by a nearly Keplerian term. The mixed variable symplectic integrators are so-called because they evaluate the planetary disturbing forces in Cartesian coordinates while using the elements to advance the orbits. Fast algorithms, like Gauss' f and g functions, exist to perform the latter task (e.g., Danby 1988; Wisdom & Holman 1991).

The orbit of any of the test particles is derived from the Hamiltonian

$$H_{\text{tp}} = H_{\text{kep}} + H_{\text{int}}. \quad (9)$$

Here, the test particle is given the first Jacobi index and the planets carry the higher Jacobi indices. As Wisdom & Holman (1991) point out, this is an advantageous choice as it gives the simplest interaction Hamiltonian. Denoting the Jacobi position of the test particle as \mathbf{x}_1 and its velocity as \mathbf{v}_1 , then

$$H_{\text{kep}} = \frac{v_1^2}{2} - \frac{k^2}{r_1}, \quad H_{\text{int}} = k^2 \sum_{i=2}^{N+1} m_i \left(\frac{\mathbf{x}_1 \cdot \mathbf{x}_i}{r_i^3} - \frac{1}{r_{1i}} \right), \quad (10)$$

where k is the Gaussian gravitational constant and N is the number of planets included in the model ($N = 8$ for our calculations). We have used the notation $r_{1i} = |\mathbf{x}_1 - \mathbf{x}_i|$ as the distance from the test particle to the i th body. As mentioned by Wisdom and Holman (1991), the intuitive interpretation of H_{int} is to note that the attraction of the Sun on the test particle equals the difference between the direct acceleration of the massive planets on the test particle and the gravitational pull of the planets on the Sun.

The most important general relativistic effects can be included by modifying the test particle Hamiltonian to

$$H_{\text{tp}} = H_{\text{kep}} + H_{\text{int}} + H_{\text{PN}}. \quad (11)$$

A clever device for incorporating the most important post-Newtonian effects into mixed variable symplectic integrators is given by Saha & Tremaine (1994). The post-Newtonian Hamiltonian is recast as

$$H_{\text{PN}} = \frac{1}{c^2} \left(\frac{3}{2} H_{\text{kep}}^2 - \frac{k^4}{r_1^2} - \frac{v_1^4}{2} \right). \quad (12)$$

The last expression contains three terms which are each integrable individually. The Keplerian part of eq. (12) can be incorporated into the usual Keplerian orbital advance using

$$\exp\left(\tau \left\{ \cdot, H_{\text{kep}} + \frac{3}{2c^2} H_{\text{kep}}^2 \right\}\right). \quad (13)$$

The Keplerian Hamiltonian is conserved with time and equals $-\frac{1}{2}k^2/a_{\text{tp}}$, a_{tp} being the semi-major axis of the test particle. After some straightforward algebra, eq. (13) becomes

$$\exp\left(\tau' \left\{ \cdot, H_{\text{kep}} \right\}\right), \quad \tau' = \left(1 - \frac{3k^2}{2c^2 a_{\text{tp}}}\right) \tau. \quad (14)$$

The second and third terms within the bracket of eq. (12) imply modifications of the test particle position and velocity before and after advancing the Keplerian orbit:

$$\frac{d\mathbf{v}_1}{dt} = -\frac{2k^4}{c^2} \frac{\mathbf{r}_1}{r_1^4}, \quad \frac{d\mathbf{x}_1}{dt} = -\left(\frac{2}{c^2} v_1^2\right) \mathbf{v}_1 \quad (15)$$

Further details of this neat formulation are given in Saha & Tremaine (1994).

3.2 The Numerical Procedure

For each of the terrestrial planets, we carry out two surveys. The first is restricted to test particles in the orbital plane of the planet. The test particles are given the same eccentricity e , inclination i , longitude of the ascending node Ω and mean

	Hyp	Mer	Ven	Ear	Mar	Jup	Tad	Hor	Total
Mercury	6	572	157	1	0	3	0	53	792
Venus	0	0	385	0	0	0	168	239	792
Earth	1	0	2	280	0	0	95	414	792
Mars	1	0	0	27	763	1	0	0	792

Table 2. Statistics for test particles in the plane of each parent planet. The second column lists the number of test particles removed from the integration because the orbit becomes hyperbolic. The next columns give the number of close encounters with each named planet. The number of survivors on tadpole and horseshoe orbits respectively are also recorded.

	Hyp	Mer	Ven	Ear	Mar	Jup	Sat	Ura	Nep	Tad	Hor	Tot
Mercury	320	558	132	40	1	33	6	1	0	??(0)	??(13)	1104
Venus	32	19	695	209	1	6	5	0	0	129	8	1104
Earth	44	0	171	669	9	7	3	0	1	182	18	1104
Mars	99	0	75	311	445	12	4	0	1	157	0	1104

Table 3. As table 2, but for test particles inclined with respect to the plane of the parent planet. There are 1104 test particles initially. The numbers terminated because their orbits become hyperbolic or because they enter the sphere of influence of any of the planet are reported. The number of survivors on tadpole and horseshoe orbits respectively are also recorded. There is some uncertainty as to the number of surviving highly inclined test particles around Mercury, as explained in the text.

anomaly M as the planet. The argument of pericentre ω is varied from 0° to 360° in steps of 5° . The initial semimajor axis is equal to the semimajor axis of the planet multiplied by a semimajor axis factor (c.f., Innanen & Mikkola’s (1989) investigation of Saturnian Trojans). The second survey is restricted to test particles with the same semimajor axis as the planet. The initial inclinations of the test particles (with respect to the plane of the planet’s orbit) are spaced every 2° and the initial arguments of pericentre are spaced every 15° . The eccentricities of the asteroids are inherited from the parent planet.

The initial conditions come from the JPL Planetary and Lunar Ephemerides, DE405 which is available at “<http://ssd.jpl.nasa.gov/>” (Chamberlain et al. 1997). The starting epoch of the integration is JED2440400.5 (28 June 1969). The standard units used for the integration are the astronomical unit, the day and the Gaussian gravitational constant $k^2 = GM_\odot$. The Earth to Moon mass ratio is $M_\oplus/M_L = 81.3$. For most of the computations described below, the timestep for Mercury is 14.27 days. The timesteps of the planets are in the ratio 1 : 2 : 4 : 8 : 8 : 64 : 64 for Mercury moving outwards, so that Neptune has a timestep of 2.5 years. The test particles all have the same timestep as Mercury. These values were chosen after some experimentation to ensure the relative energy error has a peak amplitude of $\approx 10^{-6}$ over the tens of million year integration timespans (c.f., Holman & Wisdom 1993; Saha & Tremaine 1994). Individual planetary stepsizes do introduce additional stepsize resonances and it is important to check that the resonances do not degrade the accuracy of the numerical results. Referring to Figure 3 of Wisdom & Holman (1992), the stepsize resonances begin to overlap when the ratio of semimajor axes is $\gtrsim 0.8$ and stepsize is $\gtrsim 0.2$ times the orbital period.

Bearing this in mind, it seems that the stepsize resonances are not a serious concern even for the test particles near Mercury. Nonetheless, Mercury does provide severe challenges for long-term integrations, and there is some evidence that round-off error may be affecting our results for the highly inclined test particles around Mercury.

As the test particles’ orbits are integrated, they are examined at each time step. If their trajectories become parabolic or hyperbolic orbits, they are removed from the survey. In addition, test particles which experience close encounters with a massive planet or the Sun are also terminated. The sphere of influence is defined as the surface around a planet at which the perturbation of the planet on the two-body heliocentric orbit is equal to that of the Sun on the two-body planetocentric orbit (e.g., Roy 1988). If the planet’s mass is much less than that of the Sun, this surface is roughly spherical with radius

$$r_s = a_p m_p^{2/5}, \quad (16)$$

where a_p is the semi-major axis of the planet and m_p is the planet’s mass in solar mass units. Since the algorithm we use does not allow the variable step size necessary for the treatment of close encounters, the exact size of the sphere of influence is not of great importance. Furthermore, test particles which enter the sphere of influence are typically ejected from the solar system in another 1-10 Myr (e.g., Holman 1997). In the case of the Sun, a close encounter is defined to be passage within 10 solar radii (≈ 0.005 AU). This general procedure is inherited from a number of recent studies on the stability of test particles in the Solar System (see e.g., Gladman & Duncan 1990; Holman & Wisdom 1993; Holman 1997; Evans & Tabachnik 1999)

We discuss the detailed results for each of the terrestrial

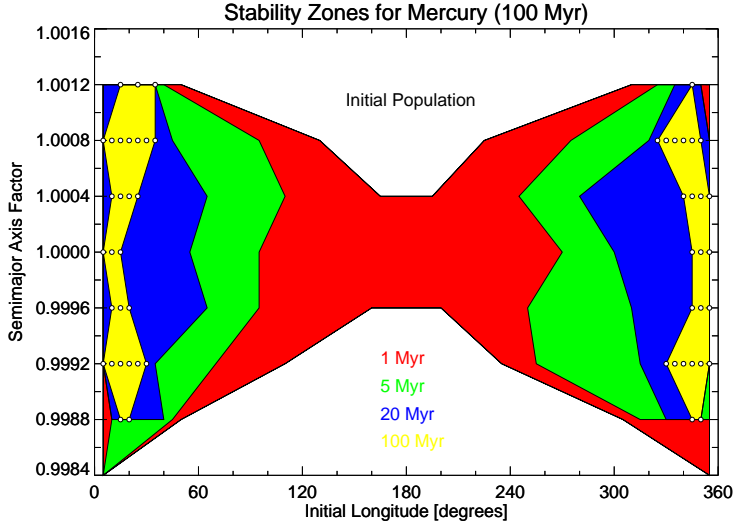


Figure 3. This shows the gradual erosion of test particles in the vicinity of the Lagrange points of Mercury. The initial population of test particles covers every 5° in longitude and every 0.0004 in semimajor axis factor. Red, green, blue and yellow mark the positions of the survivors after 1, 5, 20 and 100 million years.

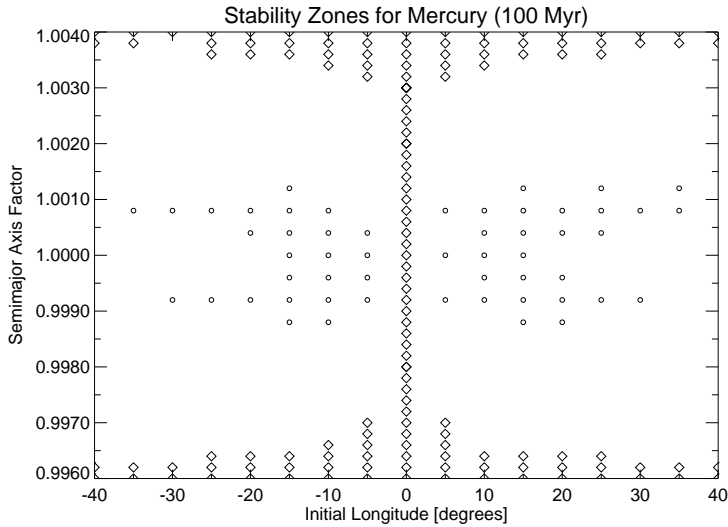


Figure 4. This shows the surviving test particles in the plane of initial longitude and semimajor axis factor marked as circles. The surviving orbits are all horseshoes. The length of integration is 100 million years. Unstable test particles in the elliptic restricted three body problem (comprising the Sun, Mercury and test particle) are shown as diamonds. Everything within the inner boundary of diamonds is stable at the level of the elliptic restricted three body problem, and so this indicates the damaging effect of perturbations from the rest of the Solar System.

planets in turn. A broad overview of the results is given in three tables. The fates of the test particles in the in-plane and inclined surveys are summarised in Tables 2 and 3 respectively. These provide the number of survivors on tadpole and horseshoe orbits, as well as the numbers suffering close encounters with each planet. Table 4 provides the average eccentricities and inclinations of the survivors at the end of the simulations.

4 MERCURIAN SURVEYS

For the Mercurian in-plane survey, the semimajor axis factor is chosen between 0.998 and 1.002 in steps of 0.0004. If the semimajor axis factor is exactly unity and the argument of pericentre is displaced by 60° or 300° , then the test particle is at the classical Lagrange point and can remain there on a stable orbit if the perturbations from the rest of the Solar System are neglected. Fig. 3 shows the time evolution of this array of test particles. The regions occupied by the test particles remaining after 1, 5, 20 and 100 million years are shown in red, green, blue and yellow respectively. After 100 million years, only 53 out of the original 792 test par-

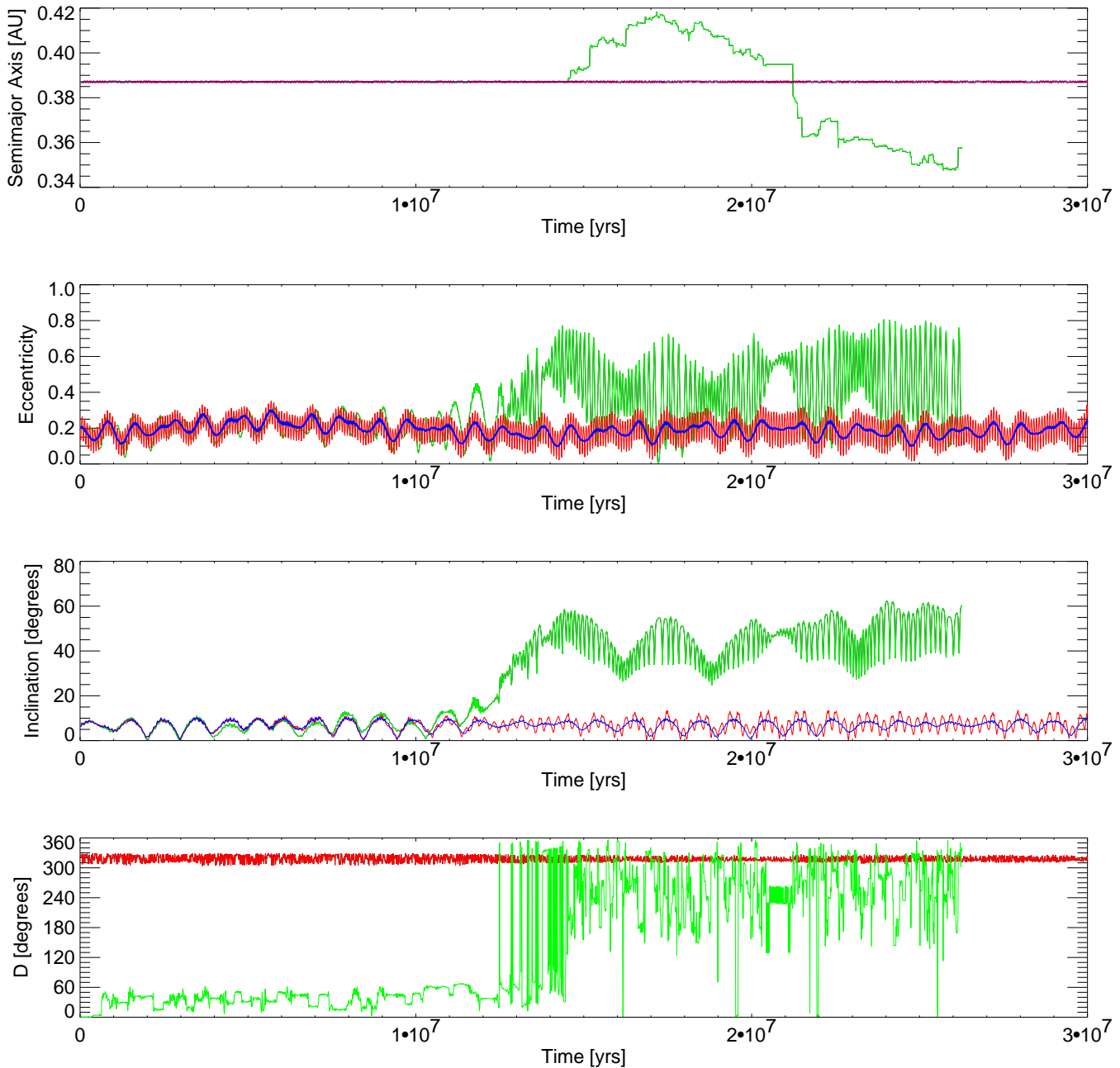


Figure 5. The first three panels of the figure show the evolution of the semimajor axis, eccentricity and inclination for Mercury (blue), a stable test particle (red) and an unstable test particle (green). The final panel shows the amplitude of libration D about the Lagrange point. Note that the stable test particle follows a horseshoe orbit, as evidenced by $D \sim 320^\circ$. The unstable test particle is initially on a tadpole orbit, then passes through a brief horseshoe phase before entering the sphere of influence of Mercury.

ticles remain. The locations of the survivors are shown in close-up in Fig. 4. The most striking point to notice is that the stable zones do not include the classical Lagrange points themselves. In fact, all the survivors follow horseshoe orbits and there are no surviving tadpole orbits. There are no long-lived Mercurian Trojans. There are two possible reasons for this. First, Mercury is the least massive of the terrestrial planets and therefore the potential wells in which any long-lived Trojans inhabit are less deep than for the other terrestrial planets. Second, Mercury is the most eccentric of the

terrestrial planets and this also encourages the erosion of the test particles. During the course of the 100 million years simulation, Mercury’s eccentricity fluctuates between ~ 0.1 and ~ 0.3 .

The top three panels of Fig. 5 show the evolution of the semimajor axis, inclination and eccentricity for Mercury, together with a stable and an unstable test particle. The distributions of the orbital elements of the survivors suggest that they belong to a low inclination, low eccentricity family of horseshoe orbits. At the end of the simulation, the aver-

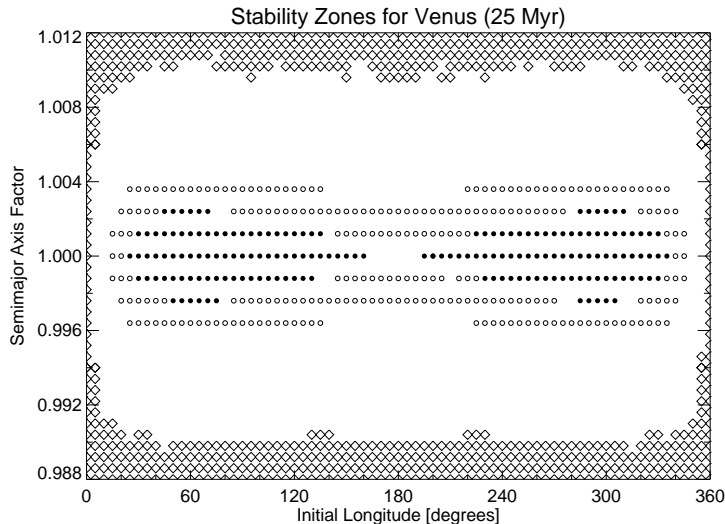


Figure 6. This shows the surviving test particles near Venus. The survivors are plotted as circles in the plane of initial longitude and semimajor axis factor. Filled circles are tadpole orbits, open circles are horseshoe orbits. Unstable test particles in the restricted three body problem comprising the Sun, Venus and asteroid are shown as diamonds. The length of integration is 25 million years.

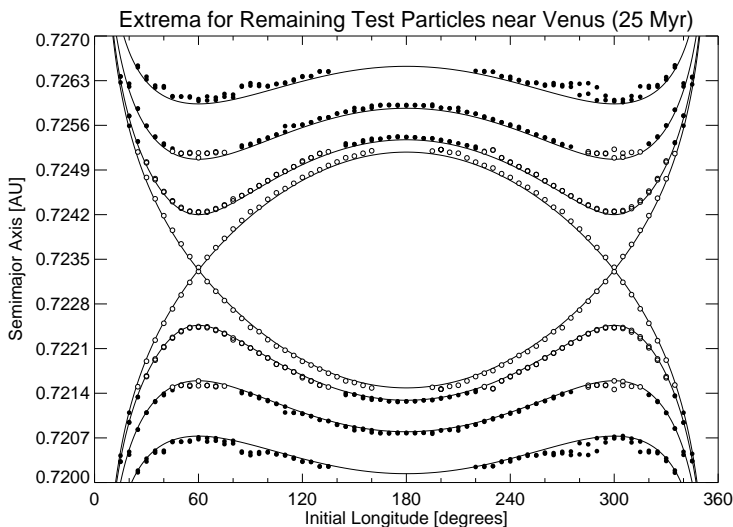


Figure 7. The extrema of the semimajor axes of the surviving test particles near Venus are plotted against their initial longitude. The extrema of tadpole orbits are shown as filled circles, the extrema of horseshoes as open circles. The extrema of survivors starting with the same semimajor axis factor fall on the same curve (eq. 19), which is drawn as a full line. This is really a consequence of the fact that the motion is derivable from an integrable Hamiltonian to an excellent approximation.

age eccentricity of the survivors is 0.186 and their average inclination is 6.968° . The lowest panel shows the evolution of the amplitude of libration D (in degrees) about the Lagrange point for the two test particles. The stable particle starts off at a semimajor axis factor of 1.001 and an initial longitude of 15° . The unstable particle starts off at exactly the L_5 Lagrange point. Notice that the eccentricity and inclination variations of the stable particle closely follow those of Mercury. The unstable test particle maintains its tadpole character only for some $\sim 1.2 \times 10^7$ years, before passing through a brief horseshoe phase for $\sim 0.5 \times 10^7$ years. After this, its semimajor axis increases to ~ 0.42 AU and finally decreases to ~ 0.35 AU before entering the sphere of influence of Mercury. The stable test particle follows a horseshoe

orbit. This is obvious on examining the lowest panel, which shows that its angular amplitude of libration about the Lagrange point is $\sim 320^\circ$.

For the Mercurian inclined survey, the orbits of 1104 test particles around Mercury are followed for 100 million years. Only thirteen test particles survived until the end of the 100 million year integration. Seven of these were low inclination ($i < 6^\circ$) test particles started off at arguments of pericentre ($\omega = 15^\circ$ or 345°) very close to that of Mercury. The remaining six survivors were all high inclination objects. On repeating these calculations on similar machines with identical roundoff, but an updated ephemerides, all six of these highly inclined orbits were terminated before the end of the 100 million years (mostly because they entered

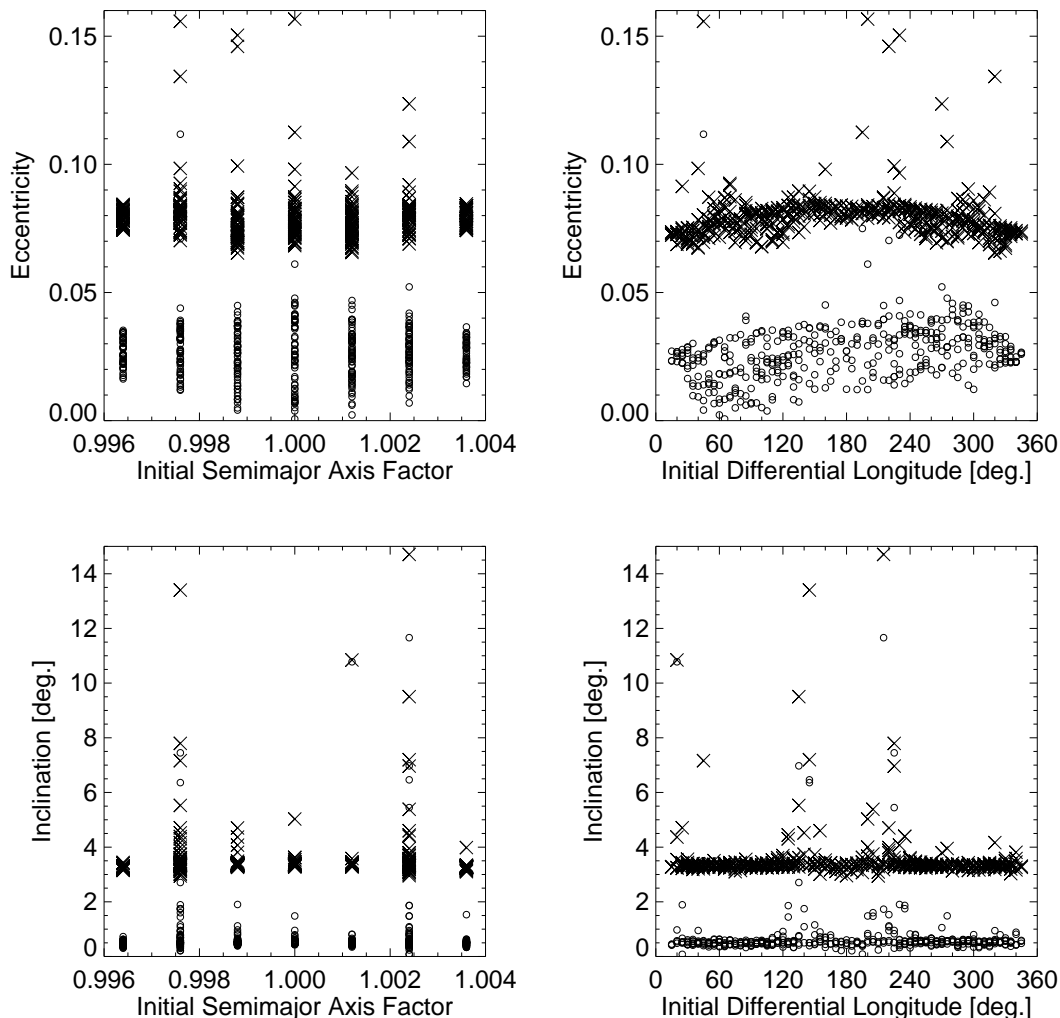


Figure 8. This shows the distributions of eccentricities and inclinations of the surviving test particles of Fig. 6 against their initial semimajor axis and longitude from Venus. In all the panels, the maximum values attained during the course of the orbit integrations are marked by crosses, the instantaneous values after 25 million years are marked by circles. The mean maximum eccentricity is 0.079, while the mean maximum inclination is 3.518° . At the end of the simulation, the average eccentricity and inclination of the sample is 0.027 and 0.706° respectively. The survivors are members of a low eccentricity and low inclination family.

the sphere of influence of Mercury), although the low inclination results were reproduced successfully. Clearly, it is not possible to draw definitive conclusions about the longevity of highly inclined asteroids near Mercury, although it seems likely that any stable zones must be small and depend sensitively on initial conditions.

5 VENUSIAN SURVEYS

Perhaps one of the likeliest planets in the inner Solar System to harbour undiscovered Trojans is Venus. Fig. 6 shows the results of the in-plane survey of Venusian test particles. The starting semimajor axes are scaled by a fraction of the planet’s semimajor axis in steps of 0.0012, while the argument of pericentre is offset from that of the planet by 5° steps. The test particles are integrated for 25 million years and the survivors recorded in the Figure. A filled circle rep-

resents a tadpole orbit, an open circle represents a horseshoe orbit. Notice that there are some long-lived survivors on horseshoe orbits even around the conjunction point. The tadpole orbits survive around L_4 for starting longitudes between 15° and 160° and around L_5 for starting longitudes between 195° and 345° . The offset in the semimajor axes of the survivors Δa compared to the parent planet a_p satisfy $\Delta a/a_p \lesssim 0.72\%$. There are 792 test particles at the beginning of the simulation, but only 407 persist till the end, of which 168 are on tadpole orbits. Horseshoes and tadpoles are of course divided by a separatrix in phase space (see Section 2). The break-up of the separatrix is associated with a chaotic layer, and this is responsible for erosion between the filled and open circles in the stable zones. At the edge of the figure, we show the stability boundary inferred from the elliptic restricted three body problem. The diamonds represent unstable test particles in the elliptic restricted three body problem (comprising the Sun, Venus and the mass-

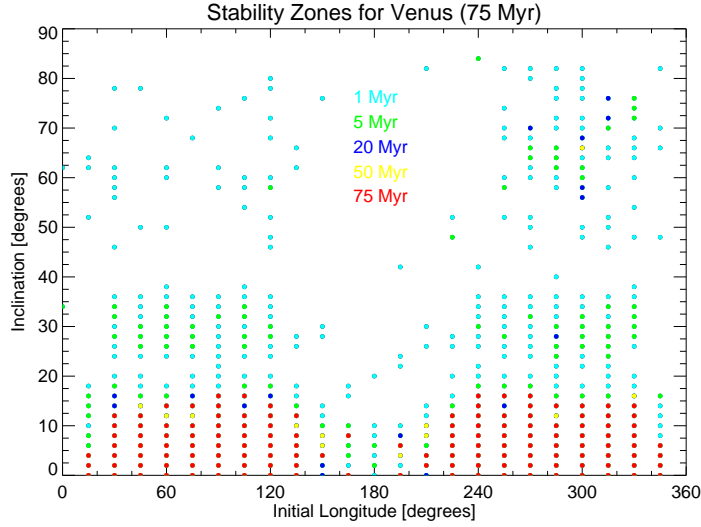


Figure 9. This shows the erosion of an ensemble of inclined test particles positioned at the same semimajor axis as the Lagrange point of Venus but varying in longitude. The test particles surviving after 5, 20, 50 and 75 million years are shown in green, blue, yellow and red respectively. Unlike the case of Mercury, there are zones of long-lived stability which hug the the line of vanishing inclination (to the plane of Venus’ orbit).

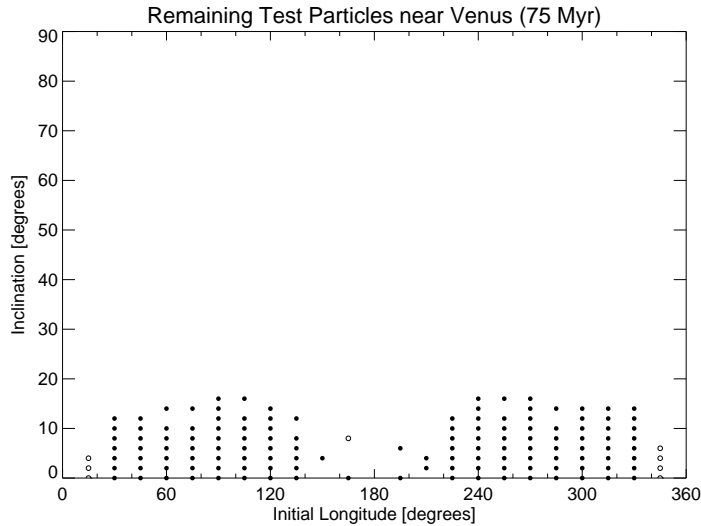


Figure 10. This shows a close-up of the stability zones of the inclined Venusian survey. Only test particles surviving the full integration time of 75 million years are plotted. The filled circles are tadpole orbits, while the open circles are horseshoe orbits. Moderate or highly inclined ($i \gtrsim 16^\circ$) Venusian asteroids are unstable, but this figure provides evidence in favour of a stable population of low inclination Venusian asteroids.

less asteroid). Everything within this outer boundary of diamonds is stable at the level of the restricted three body problem. Fig. 7 shows an at first sight surprising regularity of the orbits of the survivors. The extrema of the semimajor axis a_{ext} of the Trojan test particles are plotted against the initial longitude and fall on a one-parameter family of curves according to the semimajor axis factor. The heliocentric Hamiltonian for a test particle in the frame rotating with the mean motion of the planet may be written

$$H = -\frac{k^2}{2a} - m_p k^2 R - n_p \sqrt{(1 + m_p)a}. \quad (17)$$

Here, $n_p = \sqrt{(1 + m_p)/a_p^3}$ is the mean motion of the planet using Kepler’s third law, and R is approximated by the zeroth order term in the disturbing function

$$R = \frac{1}{a_p} \left[\frac{1}{2|\sin \frac{1}{2}\phi|} - \cos \phi \right], \quad (18)$$

where ϕ is the difference in longitude between the planet and the asteroid. This follows on setting $a = a_p$ in eq. (5). This Hamiltonian depends on time only through the slow variation of the planet’s orbital elements. These take place on a timescale much longer than the libration of the Trojan, and so the Hamiltonian is effectively constant. Expanding in the difference between the semimajor axis of the planet

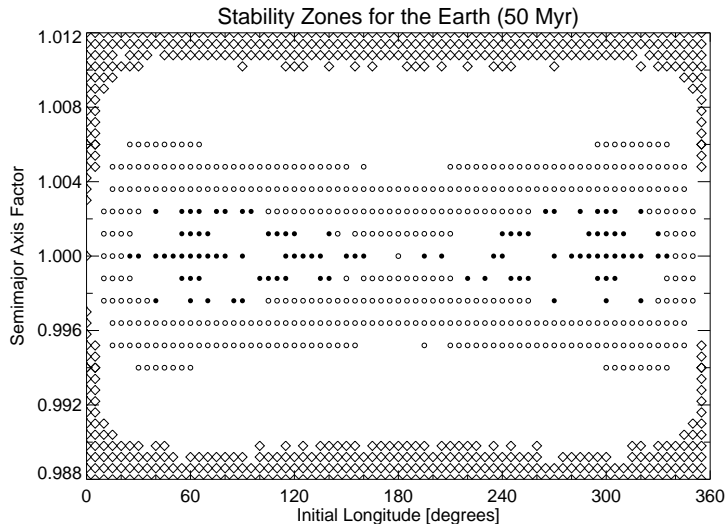


Figure 11. This shows the surviving in-plane test particles near the Earth. Filled circles are tadpole orbits, open circles are horseshoe orbits. Unstable test particles in the restricted three body problem are shown as diamonds. The length of integration is 50 million years.

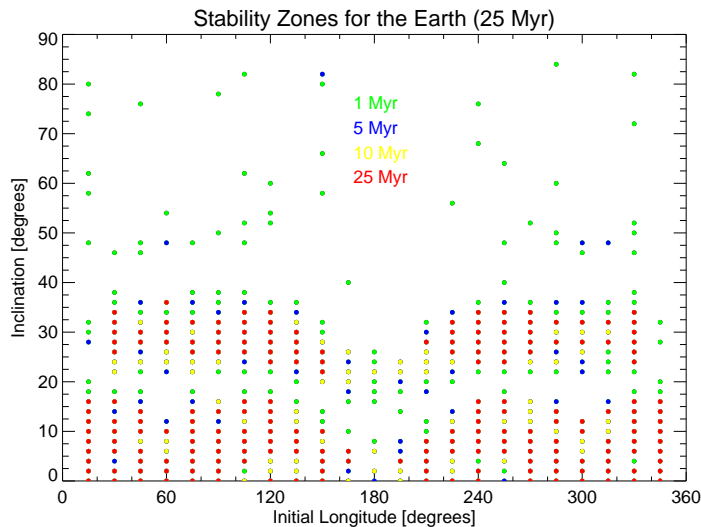


Figure 12. This shows the erosion of an ensemble of inclined test particles positioned at the same semimajor axis as the Lagrange point of the Earth but varying in longitude. The test particles surviving after 1, 5, 10 and 25 million years are shown in green, blue, yellow and red respectively.

and the Trojan, we readily deduce that a test particle with a semimajor axis factor f and which starts at a differential longitude θ has extrema a_{ext} satisfying

$$\frac{a_{\text{ext}}}{a_{\text{p}}} = 1 + \left[(f-1)^2 + \frac{8\mu}{3} \left(\frac{1}{2|\sin \frac{1}{2}\theta|} - \cos \theta - \frac{1}{2} \right) \right]^{\frac{1}{2}}, \quad (19)$$

where $\mu = m_{\text{p}}/(1+m_{\text{p}})$ is the reduced mass. The extrema of the semimajor axis of the Trojans fall on this one-parameter family of curves, as depicted in Fig. 7.

Fig. 8 shows distributions of the eccentricities and inclinations of the survivors plotted against their initial semimajor axis and longitude from Venus. In all the panels, the maximum values attained during the course of the 25 million year orbit integrations are marked by crosses, the instantaneous values are marked by circles. There are two striking

features of these diagrams. First, the eccentricities and the inclinations of the survivors remain very low indeed. The mean eccentricity of the sample after 25 million years is 0.027, while the mean inclination is 0.706° . This is a very stable family. Second, most of the survivors seem to occupy very nearly the same regions of the plots. The striking horizontal line of crosses in the rightmost panels of Fig. 8 suggest that these test particles do lie on similar orbits belonging to similar families exploring similar regions of phase space.

Fig. 9 shows the results of the Venusian inclined survey. Here, the orbits of 1104 test particles around Venus are integrated for 75 million years. The initial inclinations of the test particles (with respect to the plane of Venus' orbit) are spaced every 2° and the initial longitudes (again with respect to Venus) are spaced every 15° . The test particles are colour-coded according to whether they survive till the end

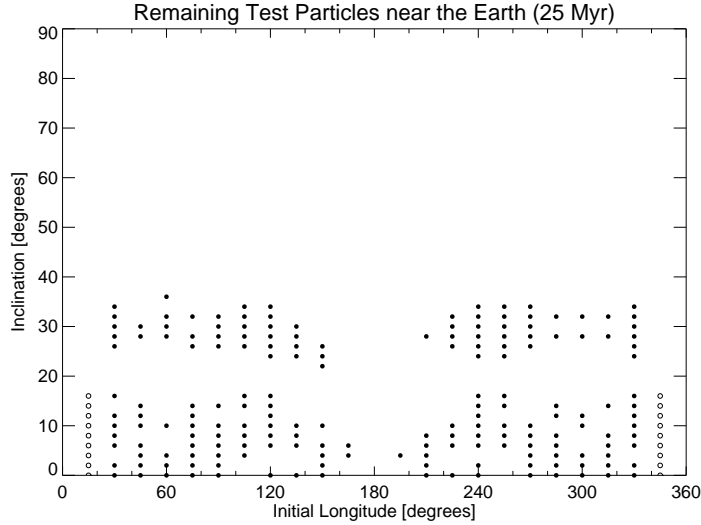


Figure 13. This shows a close-up of the stability zones of the inclined survey of terrestrial test particles. Only those surviving the full integration time of 25 million years are plotted. The filled circles are tadpole orbits, while the open circles are horseshoe orbits. There seem to be two bands of stability, one at low starting inclinations ($i \lesssim 16^\circ$) and one at moderate starting inclinations ($24^\circ \lesssim i \lesssim 34^\circ$).

Planet	$\langle e \rangle$	$\langle i \rangle$	$\langle e_{\max} \rangle$	$\langle i_{\max} \rangle$
In-plane survey				
Mercury	0.186	6.968°	0.352	13.307°
Venus	0.027	0.706°	0.079	3.518°
Earth	0.038	1.349°	0.086	3.213°
Mars	-	-	-	-
Inclined survey				
Mercury	0.400	34.069°	0.626	43.945°
Venus	0.041	6.941°	0.122	10.084°
Earth	0.064	15.778°	0.129	17.936°
Mars	0.103	25.858°	0.173	24.267°

Table 4. This lists the average eccentricity $\langle e \rangle$ and inclination $\langle i \rangle$ of the surviving test particles at the end of the simulation. Also recorded is the mean of the maxima of the eccentricities $\langle e_{\max} \rangle$ and inclination $\langle i_{\max} \rangle$ during the course of the simulation.

of the 5, 20, 50 and 75 million year integration timespans. The 137 survivors after 75 million years all have smallish inclinations ($i < 16^\circ$). Notice, too, that the stable zones around the Lagrange points are still connected by some surviving test particles at conjunction. Bodies trapped around the Lagrange points should be sought at all longitudes close to the orbital plane. Fig. 10 shows a close-up of the stable zones, with tadpole orbits represented by filled circles and horseshoe orbits by open circles. Most of the objects that do survive are true Trojans, in that their orbits are recognisably of a tadpole character. There are just 8 surviving horseshoe orbits. The ensemble has a mean eccentricity of 0.041 and a mean inclination of 6.941°.

Assuming that they are primordial, we can estimate the number of coorbiting Venusian satellites by extrapolating from the number of Main Belt asteroids (c.f., Holman 1997, Evans & Tabachnik 1999). The number of Main Belt asteroids N_{MB} is $N_{\text{MB}} \lesssim \Sigma_{\text{MB}} A_{\text{MB}} f$, where A_{MB} is the area of the Main Belt, Σ_{MB} is the surface density of the proto-planetary disk and f is the fraction of primordial objects that survive ejection (which we assume to be a universal constant). Let us take the Main Belt to be centred on 2.75 AU with a width of 1.5 AU. Fig. 6 suggests that the belt of Venusian Trojans is centred on 0.723 AU and has a width of $\lesssim 0.008$ AU. If the primordial surface density falls off inversely proportional to distance, then the number of coorbiting Venusian asteroids N_{V} is

$$N_{\text{V}} \lesssim \left(\frac{2.75}{0.723} \right) \left(\frac{0.723 \times 0.008}{2.75 \times 1.5} \right) N_{\text{MB}} \approx 0.0053 N_{\text{MB}}. \quad (20)$$

The number of Main Belt asteroids with diameters $\gtrsim 1$ km is ~ 40000 , which suggests that the number of Venusian Trojans is ~ 100 with perhaps a further ~ 100 coorbiting companions on horseshoe orbits.

6 TERRESTRIAL SURVEYS

The Earth is slightly more massive than Venus, and this augurs well for the existence of coorbiting satellite companions. The Earth has no known Trojans (Whiteley & Tholen 1998), but it does possess the asteroidal companion 3753 Cruithne which moves on a temporary horseshoe orbit (Wiegert, Innanen & Mikkola 1997; Namouni, Christou & Murray 1999). The asteroid will persist on this horseshoe orbit for a few thousand years.

Fig. 11 shows the surviving in-plane test particles near the Earth after their orbits have been integrated for 50 million years. Again, filled circles represent the tadpole orbits, open circles the horseshoe orbits. On comparison with Fig. 6, we see that the stable zones of the Earth are more extensive and the number of survivors is greater than for Venus.

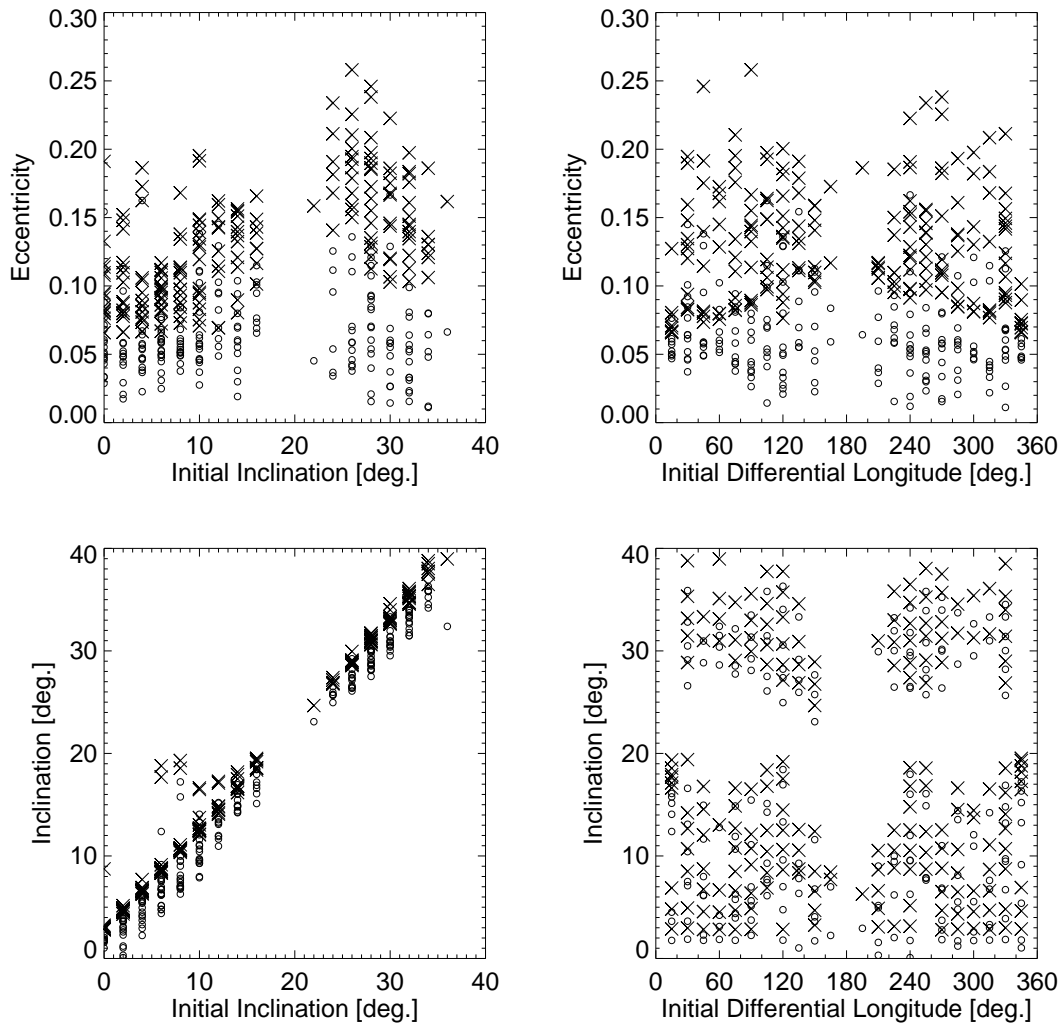


Figure 14. This shows the distributions of eccentricities and inclinations of the surviving test particles of Fig. 13 against their initial semimajor axis and longitude from the Earth. In all the panels, the maximum values attained during the course of the orbit integrations are marked by crosses, the instantaneous values after 25 million years are marked by circles. The bimodality of the inclination distribution of the survivors is manifest.

Tadpole orbits survive for $\Delta a/a_p \lesssim 0.48\%$ and horseshoes for $\Delta a/a_p \lesssim 1.20\%$. Although the number of survivors is greater, the number of true Trojans on tadpole orbits is much less than for Venus. Specifically, of the 792 original test particles, only 509 persist till the end of the simulation and of these just 95 are on tadpole orbits. In the case of the Earth, just 19% of the survivors are tadpoles, as opposed to 41% for Venus. The visual consequence of this is that the holes in the stable regions for the Earth are more pronounced than for Venus (compare also the equivalent diagram for Saturn provided by Holman & Wisdom 1993). The survivors have a mean eccentricity of 0.038 and a mean inclination of 1.349° , consistent with a long-lived population.

Fig. 12 shows the erosion of an ensemble of 1104 inclined test particles positioned at the same semimajor axis as the Earth but varying in longitude. Again, the the initial inclinations of the test particles (with respect to the plane of the Earth’s orbit) are spaced every 2° and the initial longitudes are spaced every 15° . The test particles are colour-coded

according to their survival times – those surviving after 1, 5, 10 and 25 million years are shown in green, blue, yellow and red respectively. The ensemble after 25 million years is shown in Fig. 13 with tadpoles represented as filled circles and horseshoes as open circles. Again, the first thing to note is the number of survivors – there are 200 in total, almost all of which are moving on tadpole orbits. There seem to be two bands of stability, one at low starting inclinations ($i \lesssim 16^\circ$) and one at moderate starting inclinations ($24^\circ \lesssim i \lesssim 34^\circ$). On careful inspection of our earlier Fig. 9, it is possible to discern in blue and green a similar band of stable trajectories at moderate inclination for Venus. These though are swept out much more quickly than for the Earth; they are all gone after just 5 million years. The survivors in Fig. 13 have a low mean eccentricity of 0.064. The distribution of inclinations is strikingly bimodal as is evident from Fig. 14. The mean inclination at the end of the simulation is 15.778° .

Let us remark that the Earth has more surviving test particles in both of our surveys than Venus, as well as more

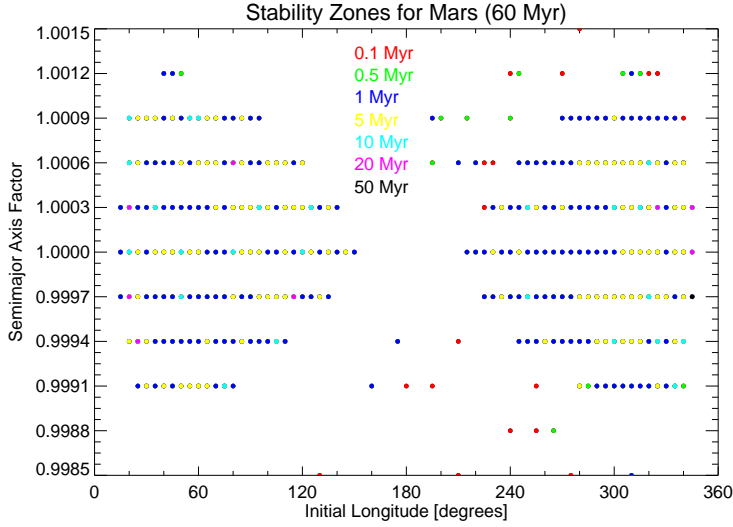


Figure 15. This shows the erosion of the in-plane test particles near Mars. There are no surviving test particles after 60 million years. The test particles are colour-coded according to their survival times.

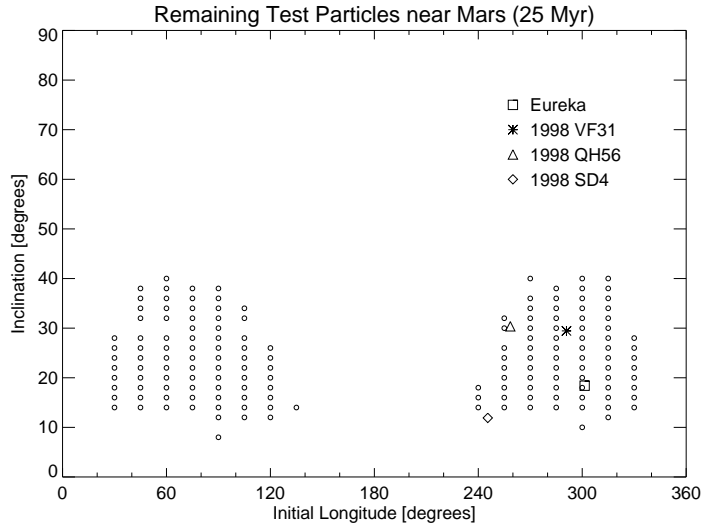


Figure 16. This shows the results of the survey of inclined test particles near Mars. The horizontal axis marks the longitude measured from Mars and the vertical axis the inclination with respect to Mars of the starting positions of test particles. Only the particles surviving till the end of the 25 million year integration are marked. Also shown are the instantaneous positions of the two Martian Trojans, namely 5261 Eureka and 1998 VF31, as well as the asteroids 1998 QH56 and 1998 SD4. The latter two have been suggested as possible Trojans, though this now seems unlikely.

extensive stable zones. This suggests that the asteroid 3753 Cruithne may not be unique, but the first member of a larger class of coorbiting terrestrial companions (Namouni, Christou & Murray 1999). Making the same assumptions as in (20), our estimate for the number of terrestrial companions is

$$N_E \lesssim \left(\frac{2.75}{1.00}\right) \left(\frac{1.00 \times 0.01}{2.75 \times 1.5}\right) N_{MB} \approx 260. \quad (21)$$

Here, we have used Fig. 11 to set the width of the stable zone around the Earth as ~ 0.005 AU. The total number of coorbiting companions will be much higher, if one includes transient objects like 3753 Cruithne.

7 MARTIAN SURVEYS

Mars is the only terrestrial planet already known to possess Trojan asteroids. These are 5261 Eureka and 1998 VF31 (see, for example, Mikkola et al. 1994, Tabachnik & Evans 1999 and the references therein). Both have moderate inclinations to the ecliptic, namely 20.3° and 31.3° respectively.

The in-plane Martian survey is presented in Fig. 15. The test particles are colour-coded according to their survival times. Most of the particles are already swept out after 5 million years. After 50 million years, there is only one test particle remaining, and it too is removed shortly afterwards. There are no survivors after 60 million years. This confirms the earlier suspicions of Mikkola & Innanen (1994)

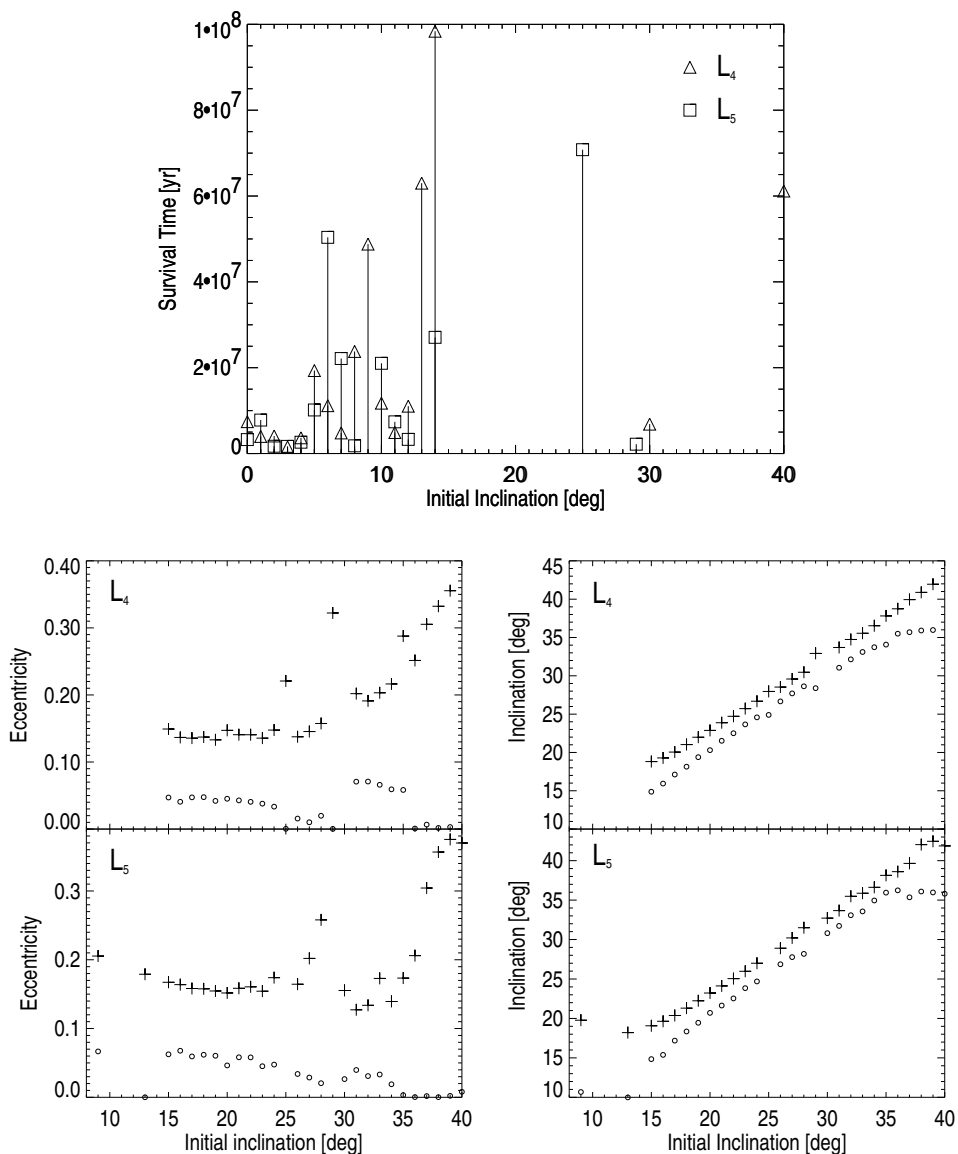


Figure 17. This upper panel shows the termination time of the 100 Myr survey of the Martian Lagrange points. Test particles at L_4 are identified by triangles while squares mark test particles at L_5 . The instantaneous (open circles) and the maximum (crosses) values of the eccentricity and inclination are illustrated in the four lower panels.

that Trojans in the orbital plane of Mars are not long-lived. As is evident from Table 2, the most common fate of the test particles is to enter the sphere of influence of Mars. The inclined survey is shown in Fig. 16, together with the positions of the two Trojans, 5261 Eureka (marked by a square) and 1998 VF31 (asterisk). Two further asteroids – 1998 QH56 (triangle) and 1998 SD4 (diamond) – have been suggested as Trojan candidates, although improved orbital elements together with detailed numerical simulations (Tabachnik & Evans 1999) now make this seem rather unlikely. The result of the inclined survey is to show stable zones for inclinations between 14° and 40° for timespans of 25 million years. The stable zones are strongly eroded at $\sim 29^\circ$.

Following this, we conducted another experiment in which inclined Martian Trojans are simulated for 100 Myrs. The initial conditions are inherited from Mars, except for the argument of pericentre which is offset by 60° (L_4) and 300° (L_5), and the inclinations which are selected in the

range from $0^\circ - 40^\circ$ from Mars’ orbital plane. To examine in more detail the effects of the other planet’s perturbations, a 1-degree step in inclination is chosen. Fig. 17 shows the results of this exercise. The upper panel expresses the termination time versus the initial inclinations of the test particles at both Lagrange points. Not surprisingly, low inclination Trojans ($i < 5^\circ$) enter Mars’ sphere of influence on a 10 million year timescale. The stable inclination windows are also recovered with a strong disturbing mechanism at 29° for L_5 and 30° for L_4 . The four lower panels give the eccentricities and inclinations of the remaining test particles at the end of the integration. Crosses identify the maximum quantities over the entire timespan, while open circles show the instantaneous values at 100 Myr. The general trend is to have stable orbits ($e_{\max} < 0.2$) in the range $15^\circ - 34^\circ$ in the case of L_4 and $9^\circ - 36^\circ$ in the case of L_5 . Interestingly, the two securely known Trojans, namely 5261 Eureka and

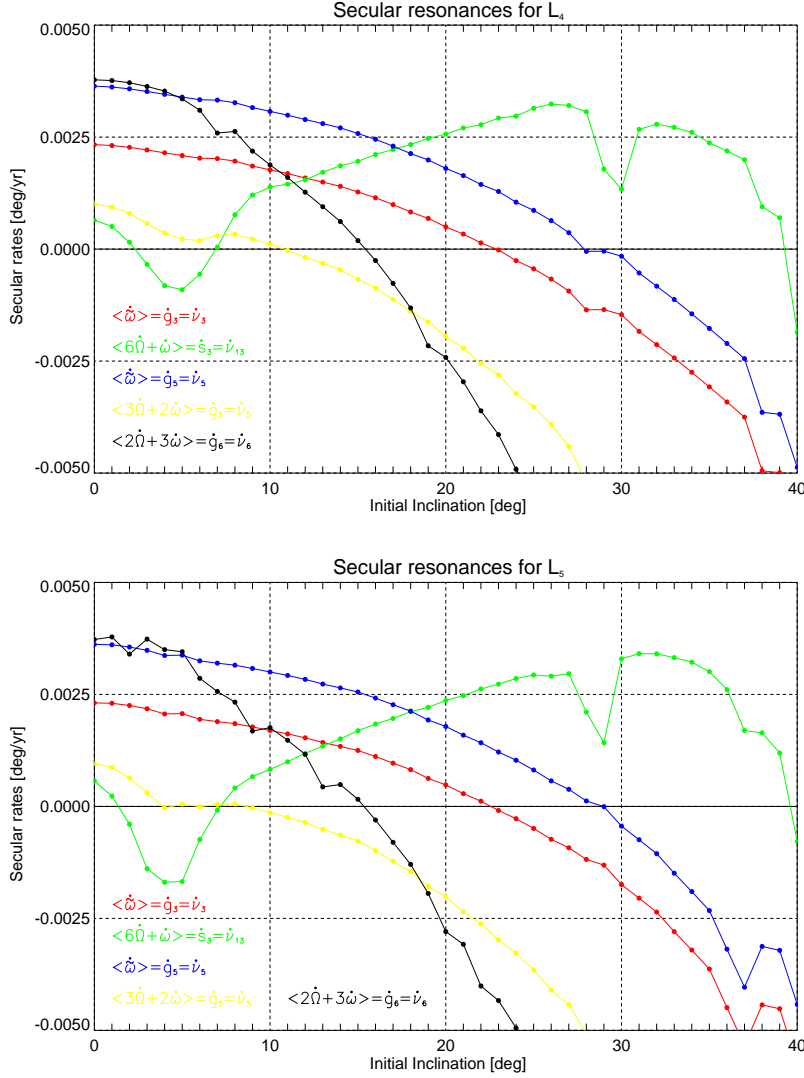


Figure 18. This shows the locations of the principal secular resonances for the L_4 and L_5 points of Mars. The rates of change of the angles (in degrees per year) are plotted against inclination. Resonances occur when these curves cross the horizontal axis of zero rate of change. Notice the strong linear resonance with Jupiter (blue curve). This occurs at $\sim 28 - 30^\circ$ at the L_4 point and at $\sim 29^\circ$ at the L_5 point. Many of the low inclination test particles are destabilised by the non-linear Jovian resonance (yellow curve), which persists over a range of inclinations between $\sim 6 - 11^\circ$. There are weaker resonances with the Earth (red and green curves) as well as Saturn (black curve).

1998 VF31, occupy positions at L_5 corresponding to the two local minima of the maximum eccentricity curve.

The results for the inclined Martian Trojans are unusual, and it is natural to seek an explanation in terms of secular resonances. Large disturbances can occur when there is a secular resonance, that is, when the averaged precession frequency of the asteroid's longitude of pericentre $\langle \dot{\omega} \rangle$ or longitude of node $\langle \dot{\Omega} \rangle$ becomes nearly equal to an eigenfrequency of the planetary system (e.g., Brouwer & Clemence 1961; Williams & Faulkner 1981; Scholl et al. 1989). The secular precession frequencies in linear theory are usually labelled g_j and s_j ($j = 1, \dots, 8$ for Mercury to Neptune) for the longitude of pericentre and longitude of node respectively. Their mean values computed over 200 million years are listed in Laskar (1990).

Fig. 18 can be used to infer the positions of some of the principal secular resonances as a function of inclination in the vicinity of each Lagrange point. The vertical axis is

the rate of variation of various angles, the horizontal axis is the inclination. A resonance occurs whenever the rate of variation vanishes. The blue curve shows the frequency $\langle \dot{\omega} \rangle - g_5$, which vanishes at inclinations $\sim 28 - 30^\circ$ for the L_4 point and 29° at the L_5 point. Notice that the resonance is much broader at the L_4 point. The yellow curves show $\langle 3\dot{\Omega} + 2\dot{\omega} \rangle - g_5$. This frequency vanishes at a range of inclinations between $\sim 6 - 11^\circ$, again with slight differences noticeable at the two Lagrange points. As these are resonances with Jupiter, they are expected to be the most substantial. At this semimajor axis, there is just one resonance with Saturn. The black curves show the frequency $\langle 2\dot{\Omega} + 3\dot{\omega} \rangle - g_6$. This resonance occurs at inclinations of $\sim 15^\circ$. Lastly, there are two weaker resonances with the Earth. These may be tracked down using the red curve, which shows $\langle \dot{\omega} \rangle - g_3$, and the green curve, which shows $\langle 6\dot{\Omega} + \dot{\omega} \rangle - s_3$. This completes the list of the main resonances in the vicinity of Mars. The

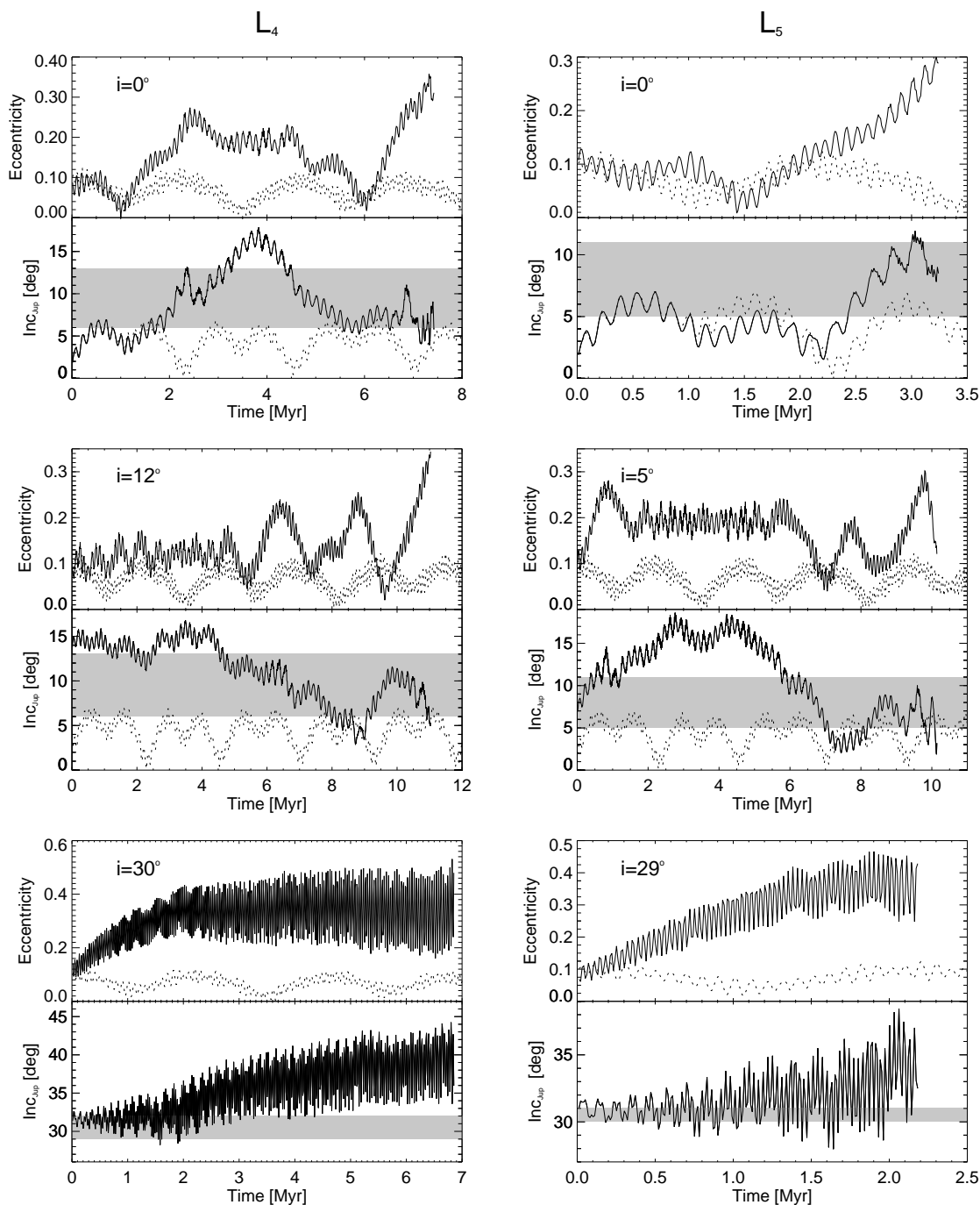


Figure 19. This shows the evolution of the inclination (with respect to the plane of Jupiter) and the eccentricity of selected orbits in full lines. The behaviour of Mars is shown in a broken line. The inclinations over which the two Jovian resonances operate are shown as shaded grey bands. The left column refers to L_4 , the right column to L_5 . In each case, the starting inclination with respect to the plane of Mars is noted in the panel.

importance of the Jovian resonances in particular has been pointed out before by Mikkola & Innanen (1994).

Fig. 19 illustrates the evolution of a few arbitrarily selected orbits. The left panels refer to the L_4 Lagrange point, the right panels to the L_5 point. The panels are labelled according to the initial inclination with respect to Mars' orbit. They plot the evolution of the eccentricity e and the inclination with respect to Jupiter i_{jup} for a typical test particle (full curve) and Mars (broken curve). The inclinations over which the two Jovian resonances operate are shown as

shaded bands. The uppermost two panels refer to orbits that start out in the orbital plane of Mars. Their inclination is initially increased, and this takes the orbits into the régime in which one of the Jovian resonances is dominant. The eccentricity of the orbit is pumped whenever it lingers in the shaded inclination band. This makes the orbit Mars-crossing and the test particle is terminated. The middle two panels show the fates of orbits at intermediate inclinations of 12° at the L_4 point and 5° at the L_5 point. Although the behaviour is quite complex, the final increase in eccentricity

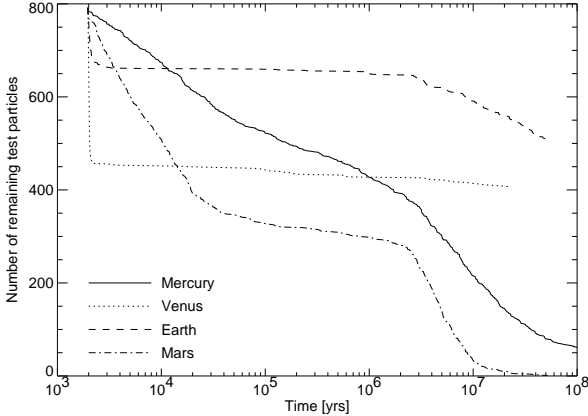


Figure 20. The number of remaining test particles is plotted against time for our in-plane surveys of the Lagrange points of the four terrestrial planets. The extrapolations presented in Table 5 suggest that there will be some hundreds of surviving test particles for Venus and the Earth even if the simulations are continued for the age of the Solar System (~ 5 Gyrs).

in both cases coincides with prolonged stays in the resonant region. We conclude that the low inclinations test particles are destabilised by this secular resonance with Jupiter. The bottom two panels show fates of test particles starting off at 30° at the L_4 point and 29° at the L_5 point. In both cases, there is a rapid and pronounced increase in the eccentricity, which takes it onto a Mars-crossing path. This destabilisation occurs only for a very narrow range of inclinations. This is manifest in the erosion in Fig. 16, especially at the L_4 point near inclinations of 30° .

Mikkola & Innanen (1994) suggested that the instability of low inclination Martian Trojans was due to a secular resonance with Mars driving the inclination upwards. In their picture, this continues until a critical inclination of $\sim 12^\circ$ is reached when $3\Omega + 2\dot{\omega}$ resonates with Jupiter. The difficulty with this is that it is not clear whether the claimed Martian secular resonance – which is really just equivalent to the statement that the test particle is coorbiting – is responsible for the inclination increase. Our Fig. 18 seems to show that $\langle 3\Omega + 2\dot{\omega} \rangle - g_5$ nearly vanishes over a broad range of inclinations and we suspect it may be able to cause the damage on its own.

8 CONCLUSIONS

The possible existence of long-lived coorbiting satellites of the terrestrial planets has been examined using numerical simulations of the Solar System. Of course, integrations in the inner Solar System are laborious as much smaller timesteps are required to follow the orbits of the satellites of Mercury as opposed to the giant planets like Jupiter. Our numerical surveys have been pursued for timescales up to 100 million years – typically an order of magnitude greater than previous computations in the inner Solar System. The numerical algorithm is a symplectic integrator with individual timesteps that incorporates the most important post-Newtonian corrections (Wisdom & Holman 1991; Saha & Tremaine 1994).

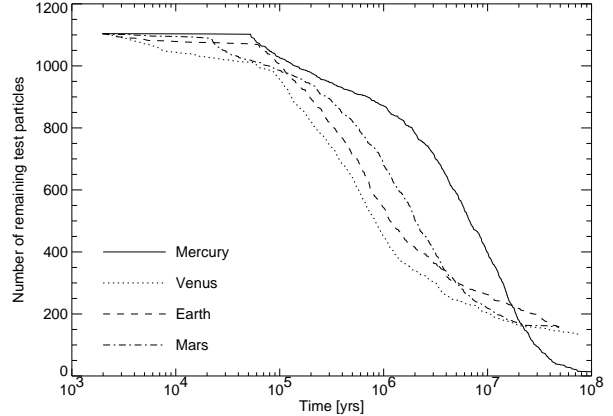


Figure 21. As Fig. 20, but for our surveys of inclined orbits near the Lagrange points of the four terrestrial planets. The decay laws for test particles around all four planets are similar and they are not well-fit by a logarithmic decay law.

One worry concerning our integrations is that they extend at most to 100 million years, which is a small fraction of the age of the Solar System (~ 5 Gyrs). To gain an idea of the possible effects of longer integration times, we can use the approximate device of fitting our existing data and extrapolating. Graphs of the number of surviving particles against time are shown in Figs. 20 - 21 for the in-plane and inclined surveys respectively. In the former case, the data are generally well-fit by a logarithmic decay law of form

$$N(t) = a + b \log_{10}(t[\text{yrs}]) \quad (22)$$

Table 5 shows the best fitting values of a and b . It also gives the extrapolated number of test particles after 1 and 5 Gyrs. For both Venus and the Earth, this suggests that several hundred test particles remain, even if the simulations are run for the age of the Solar System. In the inclined case, the data is not well-fitted by logarithmic decay laws. Instead, Table 6 gives the results of fitting the data between 10 and 100 Myr to a power-law decay of form

$$N(t) = \frac{10^c}{(t[\text{yrs}])^d} \quad (23)$$

Extrapolation suggests that some inclined test particles remain for Venus, the Earth and Mars even after 5 Gyr. However, these numbers are highly speculative for the inclined survey, as only the tail of the distribution is fitted.

The results of our surveys for Venus and the Earth are somewhat similar. Long-lived coorbiting satellites can persist in the orbital planes of both planets. The stable zones of the Earth are larger than those Venus, although the Earth retains fewer true Trojans or tadpoles. The semi-major axes of the stable test particles a , as compared to the parent planet a_p , satisfy $\Delta a/a_p \lesssim 0.72\%$ for Venus and $\Delta a/a_p \lesssim 1.2\%$ for the Earth. Both Venus and the Earth have low inclination régimes in which long-lived test particles survive for timescales of tens of millions of years, despite the disturbing perturbations from the remainder of the Solar System. The stable zones satisfy $i \lesssim 16^\circ$ for Venus. For the Earth, there are two bands of stability, one at low

Planet	a	b	$N(3000 \text{ yrs})$	$N_{\text{exp}} (1\text{Gyr})$	$N_{\text{exp}} (5\text{Gyr})$
Mercury	1283.2 ± 5.3	-150.6 ± 0.89	756	–	–
Venus	503.5 ± 1.9	-12.61 ± 0.33	456	390	381
Earth	946.8 ± 18.8	-52.36 ± 2.71	663	476	439
Mars	1089.6 ± 8.2	-142.33 ± 1.53	691	–	–

Table 5. For each planet, the data on the number of surviving in-plane test particles $N(t)$ is fitted for $t > 3000$ yr. The parameters a and b in the logarithmic fits are listed in the second and third columns. The last two columns of the tables give the extrapolated number of test particles estimated to remain after 1 Gyr and 5 Gyr.

Planet	c	d	$N (10 \text{ Myr})$	$N_{\text{exp}} (1\text{Gyr})$	$N_{\text{exp}} (5\text{Gyr})$
Mercury	13.89 ± 0.07	1.60 ± 0.01	396	–	–
Venus	3.62 ± 0.03	0.19 ± 0.005	203	80	59
Earth	4.61 ± 0.03	0.31 ± 0.005	262	63	38
Mars	4.037 ± 0.1	0.25 ± 0.014	217	67	45

Table 6. For each planet, the data on the number of surviving inclined test particles $N(t)$ is fitted for $10 < t < 100$ Myr. The parameters c and d in the power-law fits are listed in the second and third columns. The last two columns of the tables give the extrapolated number of test particles estimated to remain after 1 Gyr and 5 Gyr.

inclinations ($i \lesssim 16^\circ$) and one at moderate inclinations ($24^\circ \lesssim i \lesssim 34^\circ$). However, there is a hint that the higher inclination band may be further eroded with still longer timespan integrations. The inclined test particles that survive primarily move on tadpole orbits. It is possible to make very crude estimates of numbers by extrapolation from the Main Belt. These suggest that there may be some hundreds of asteroids in the coorbital regions of Venus and the Earth.

In the case of Mercury, very few of the test particles – whether starting in the orbital plane or at higher inclinations – survive till the end of the integrations. This seems reasonable, as both the low mass and the high eccentricity of Mercury militate against stable zones. A population of numerous, long-lived Mercurian Trojans seems rather unlikely. Recently, Namouni et al. (1999) have speculated that highly inclined coorbiting Mercurian satellites (“Vulcanoids”) may exist. Our survey does hint at the survival of a handful of test particles at high inclinations. On re-simulating these results over the same timespan using an updated ephemerides, these test particles did not survive but were ejected. So, if there are stable zones of inclined coorbiting satellites, then they must be narrow and rather sensitive to the detailed initial conditions.

From the viewpoint of dynamics, Mars offers perhaps the greatest interest of all. Here, the test particles within the orbital plane are all ejected on 60 million year timescales. The inclined survey shows stable zones for inclinations between 14° and 40° . This is certainly consistent with the two known Martian Trojans (5261 Eureka and 1998 VF31) which have orbits moderately inclined to the ecliptic (20.3° and 31.3° respectively) about the L_5 point. The survey shows strong erosion at a narrow band of inclinations concentrated around $\sim 28 - 30^\circ$ at L_4 and 29° at L_5 . This may be traced to a strong, but narrow, Jovian resonance. The averaged precession frequency of the test particle’s longitude of pericentre $\langle \dot{\varpi} \rangle$ is equal to the secular precession frequency of the longitude of pericentre of Jupiter g_5 . We believe that the destabilisation of the low inclination and in-plane orbits

is also due to Jupiter. Here, the combination of frequencies $(3\Omega + 2\dot{\omega}) - g_5$ vanishes over a broad range of inclinations between $\sim 6 - 11^\circ$. As they evolve, low inclination test particles enter this band of inclinations, their eccentricity is increased and they become Mars-crossing.

ACKNOWLEDGMENTS

NWE is supported by the Royal Society, while ST acknowledges financial help from the European Community. We wish to thank John Chambers, Jane Luu, Seppo Mikkola, Fathi Namouni, Prasenjit Saha and Scott Tremaine for helpful comments and suggestions. Jane Luu and Prasenjit Saha provided critical readings of the manuscript.

REFERENCES

- Brouwer D., Clemence G.M. 1961, *Methods of Celestial Mechanics* (Academic Press, New York)
- Brown E.W., Shook C.A. 1933, *Planetary Theory* (Cambridge University Press, Cambridge)
- Danby J.M.A. 1988, *Fundamentals of Celestial Mechanics* (Willmann-Bell, Richmond)
- Érdi B. 1997, *Cel. Mech.*, 65, 149
- Evans N.W., Tabachnik S. 1999, *Nature*, 399, 41
- French L.M., Vilas F., Hartmann W.K., Tholen D.J. 1989, In “Asteroids II”, eds Binzel R.P., Gehrels T., Matthews M.S., p. 468, (Tucson, University of Arizona Press)
- Gladman B., Duncan M. 1990, *AJ*, 100, 1680
- Holman M.J. 1997, *Nature*, 387, 785
- Holman M.J., Wisdom J. 1993, *AJ*, 105, 1987
- Holt H.E., Levy D. 1990, *IAU Circular No.* 5045
- Innanen K., Mikkola S., 1989, *AJ*, 97, 900
- Kinoshita H., Yoshida H., & Nakai H., 1991, *Cel. Mech.*, 50, 59
- Lagrange J.L., 1772, *Oeuvres de Lagrange*, tome VI, 229
- Laskar J., 1990, *Icarus*, 88, 266
- Mikkola S., Innanen K.A. 1990, *AJ*, 100, 290
- Mikkola S., Innanen K.A. 1992, *AJ*, 104, 1641

- Mikkola S., Innanen K.A., Muinonen K., Bowell E. 1994, *Cel. Mech.*, 58, 53
- Mikkola S., Innanen K.A. 1994, *AJ*, 107, 1879
- Mikkola S., Innanen K.A. 1995, *Earth, Moon and Planets*, 71, 195
- Namouni F., 1999, *Icarus*, 137, 293
- Namouni F., Christou A.A., Murray C.D., 1999, *Phys. Rev. Lett.*, 83, 2506
- Namouni F., Murray C.D., 1999, *Cel. Mech.*, submitted
- Pars L.A. 1965, *A Treatise on Analytical Dynamics* (Heinemann, London)
- Plummer H.C. 1960, *An Introductory Treatise on Dynamical Astronomy* (Dover, New York)
- Quinn T.R., Tremaine S.D., Duncan, M. 1991, *AJ*, 101, 2287
- Roy A.E. *Orbital Motion* (Hilger, Bristol, 1988)
- Saha P., Tremaine S. 1994, *AJ*, 108, 1962
- Scholl H., Froeschlé Ch., Kinoshita H., Yoshikawa M., Williams J.G., 1989, In “Asteroids II”, eds Binzel R.P., Gehrels T., Matthews M.S., p. 845, (Tucson, University of Arizona Press)
- Shoemaker E.M., Shoemaker C.S., Wolfe R.T. 1989, In “Asteroids II”, eds Binzel R.P., Gehrels T., Matthews M.S., p. 468, (Tucson, University of Arizona Press)
- Smith B.A. et al. 1982, *Science*, 215, 504
- Tabachnik S.A., 1999, D. Phil. thesis, Oxford University (see “<http://www-thphys.physics.ox.ac.uk/users/Galactic/science/dphil.html>”)
- Tabachnik S.A., Evans N.W. 1999, *ApJ*, 517, L63
- Wiegert P.A., Innanen K., Mikkola S., *Nature*, 387, 685
- Whiteley R.J., Tholen D.J. 1998, *Icarus*, 136, 154
- Whittaker E.T. 1904, *Analytical Dynamics* (Cambridge University Press, Cambridge)
- Williams J.G., Faulkner J. 1989, *Icarus*, 46, 390
- Winiarski M. 1989, *Earth, Moon and Planets*, 47, 193
- Wisdom J., Holman M.J. 1991, *AJ*, 102, 1528
- Wisdom J., Holman M.J. 1992, *AJ*, 104, 2022
- Yoder C.F., Colombo G., Synnott S.P., Yoder K.A. 1983, *Icarus*, 53, 431
- Yoder C.F., Synnott S.P., Salo H. 1989, *AJ*, 98, 1875
- Zhang S.-P., Innanen K.A. 1988a, *AJ*, 96, 1983
- Zhang S.-P., Innanen K.A. 1988b, *AJ*, 96, 1989
- Zhang S.-P., Innanen K.A. 1988b, *AJ*, 96, 1995

We are indebted to Seppo Mikkola, who kindly confirmed the correctness of these expressions for us. The formula given in Mikkola et al. (1994) is erroneous. Expansions to the fourth order in both eccentricity and inclination are presented in Tabachnik (1999).

APPENDIX A: AUXILIARY FORMULAE

This appendix lists auxiliary functions for the averaged disturbing function

$$\begin{aligned}
 U_{2,0} &= \frac{a}{a_p} \left[\frac{1}{2}(e^2 + e_p^2) \cos \phi - ee_p \cos(\omega + \Omega + 2\phi) \right] \cos^2 \frac{i}{2}, \\
 U_{2,3} &= \left[\frac{1}{4}ee_paa_p \cos(\omega + \Omega + 2\phi) - \frac{1}{2}(e^2 + e_p^2)aa_p \cos \phi \right. \\
 &\quad \left. + \frac{9}{4}ee_paa_p \cos(\omega + \Omega) \right] \cos^2 \frac{i}{2} - \frac{3}{4}(a^2e^2 + a_p^2e_p^2), \\
 U_{2,5} &= \left[\frac{15}{8}(e^2 + e_p^2)a^2a_p^2 + \frac{27}{8}ee_p a^2a_p^2 \cos(\omega + \Omega - \phi) \right. \\
 &\quad \left. - \frac{9}{4}ee_p a^2a_p^2 \cos(\omega + \Omega + \phi) - \frac{9}{8}(e^2 + e_p^2)a^2a_p^2 \cos 2\phi \right. \\
 &\quad \left. + \frac{3}{8}ee_p a^2a_p^2 \cos(\omega + \Omega + 3\phi) \right] \cos^4 \frac{i}{2} + \\
 &\quad \left[\frac{3}{4}ee_paa_p(a^2 + a_p^2) \cos(\omega + \Omega + 2\phi) - \frac{3}{2}aa_p(a^2e^2 + \right. \\
 &\quad \left. a_p^2e_p^2) \cos \phi - \frac{9}{4}ee_paa_p(a^2 + a_p^2) \cos(\omega + \Omega) \right] \cos^2 \frac{i}{2} \\
 &\quad + \frac{3}{4}(a^4e^2 + a_p^4e_p^2) + \frac{3}{2}ee_p a^2a_p^2 \cos(\omega + \Omega + \phi) \\
 &\quad + \frac{3}{4}a^2a_p^2 \sin^4 \frac{i}{2}
 \end{aligned}$$